

Electrochemical and Microstructural Investigations of AA6063 Friction Stir Welded Joint

F. Jafari^a, M. R. Khanzadeh Gharah Shiran^b, Z. Bakhtiari^c, M. Akbari^d,
Y. Shajari^e, Z. S. Seyedraoufi^f, and H. Bakhtiari^{e,*}

^aDepartment of Materials Engineering, Shahreza Branch Islamic Azad University, Isfahan, Iran

^bCenter for Advanced Engineering Research, Majlesi Branch, Islamic Azad University, Isfahan, Iran

^cFaculty of Metallurgical Engineering, Arak University, Arak, Iran

^dFaculty of Mining and Metallurgical Engineering, Amirkabir University of Technology, Tehran, Iran

^eMaterials and Energy Research Center, Karaj, 14155-4777 Iran

^fDepartment of Metallurgy and Materials Engineering, Karaj Branch, Islamic Azad University, Karaj, Iran

*e-mail: hamid.bakhtiari60@gmail.com

Received November 6, 2018; revised March 11, 2019; accepted March 25, 2019

Abstract—In the present study, the influence of the pin rotating speed on corrosion behavior and mechanical properties of the friction stir welded (FSW) 6063 aluminum alloy joints was investigated. The welding process was performed at rotating speeds of 800, 1000, and 1200 rpm and a constant traverse speed of 50 mm/min. The joints were analyzed via optical microscopy, scanning electron microscopy, and microhardness test. A cyclic polarization test and electrochemical impedance spectroscopy (EIS) were performed so as to study the effect of the pin rotating speed on corrosion behavior of joints in the solution of sodium chloride (3.5%). Microhardness results showed that the maximum amount of hardness is related to the sample with 1000 rpm rotating speed because of optimized input heat, which caused an increase in the grain refinement and dynamic recrystallization. The cyclic polarization test demonstrated that the corrosion rate in the heat affected zone (HAZ) was higher than that of the base and weld metals; this is due to grain coarsening and an increase of secondary phase particles, which causes intensification of galvanic corrosion. It was found that the higher the pin rotating speed, the higher the corrosion rate. The growth of secondary phase particles was identified due to an input heat increase. Also, EIS results indicated that increasing the pin rotating speed at FSW reduces the polarization resistance (R_p) amount at the Nyquist diagram, followed by a decrease of corrosion resistance. A lower amount of R_p and corrosion resistance verified in the HAZ was compared to those of the weld metal.

Keywords: friction stir welding, 6063 aluminum alloy, pin rotating speed, cyclic polarization test, electrochemical impedance test

DOI: 10.3103/S1068375520010093

INTRODUCTION

Aluminum alloys have a low strength to weight ratio, good plasticity, and desirable strength. Also, they possess acceptable corrosion resistance. Aluminum alloys of 6000 series are the most applicable among standard alloys due to their technical and economical properties. Good weldability, excellent corrosion resistance and anodizing effects as well as a middle capacity of machinability are the distinguishing properties of this series of alloys.

As regards fusion welding methods, they have such usual defects as inclusions, cracking at the weld area, and tensional residual stresses, so their applications in joining of alloys have been limited to practically sensible applications. The friction stir welding (FSW) method as a reliable route lacking those defects just

mentioned; this is why it has been widely utilized to join aluminum alloys and other metals like copper, titanium, magnesium, and steel [1–6]. This method is used in industrial sensitive applications such as aircraft, aerospace, automobile, railway, and shipbuilding. It has the ability to weld thin and thick sheets in a range of 0.5–50 mm at a single step and thicker parts (to 75 mm) by a two-step process.

Since the FSW is a solid-state process, welding is performed at temperatures lower than melting points of materials, so usual defects in fusion welding have been removed from this process and the mechanical properties and corrosion behavior of the weld metal would be modified and improved. Although the joining process in this method is performed at lower temperatures of the base metal melting point, the resultant heat may change the alloy structure and finally the

Table 1. Chemical composition of 6063 aluminum alloy (wt %) used in the study

El.	Al	Fe	Cr	Cu	Si	Mn	Mg	Ti
Wt %	Base	0.35	0.10	0.10	0.43	0.10	0.83	0.09

corrosion behavior would be affected. Change and modifications of microstructure for this welding route relate to the dynamic recrystallization process due to friction heat and intense plastic deformation [1–6].

Mechanical behavior of the FSW samples is affected by the chemical composition of an alloy and input heat. Hardness changes in the range of heat treatable aluminum alloys is affected by alloy tempering conditions, grain size, and density of an alloy [6–8].

The authors in [9] indicated that the recrystallized grain size increased exponentially by raising the temperature and the grain size, which caused hardening of the weld metal in FSW.

Generally, resultant microstructures of FSW include four distinct areas: the central area of the weld metal labeled as the weld or stir zone, the heat affected zone (HAZ), the thermo-mechanically affected zone (TMAZ) and the base metal. The base metal is not affected by cyclic heat and plastic deformation and the heat amount of this zone is not enough to change the base metal microstructure. Since each of these zones has different micro-structures, their changes can cause distinct corrosion behaviors for welded work pieces [1–5].

It was shown elsewhere that if the surface of the work piece gets smoother at a high traverse speed of FSW, then grain deformation increases thus causing lower residual stress [10]. Other researchers studied

the corrosion behavior of 6061 aluminum alloy by using the immersion method and electrochemical test. Their results demonstrated that both the HAZ and TMAZ were more sensitive to grain boundary corrosion due to the presence of magnesium-rich deposition phase at the inside of grain boundaries [11]. They have also investigated the pitting and grain boundary corrosion resistance of FSWed 6061 T6 aluminum alloy [12] and found that the HAZ was sensitive to both of the mentioned corrosion kinds and the corrosion resistance of this zone was lower than that of other zones due to lacking of copper areas at grain boundaries of the HAZ.

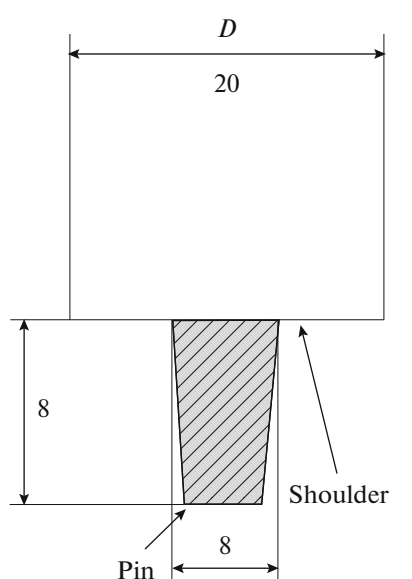
The aim of this paper was to evaluate the pin rotating speed effect on corrosion behavior, mechanical properties, and microstructure of the AA6063 joints.

MATERIALS AND METHODS

A 15 mm sheet of 6063 aluminum alloy was used in the dimensions of $20 \times 5 \text{ cm}^2$. The chemical composition of AA6063 was as given in Table 1. The pin used in the welding process was a kind of hot working steel with the hardness of 48 C Rockwell. The pin shoulder diameter, its length and diameter were 20, 8, and 8 mm, respectively, which is presented in Fig. 1. The annealed 6063 T6 aluminum alloy sheets were put in a butt form after washing by acetone and welded from both sides. This process was operated at three different rotating speeds of 800, 1000, and 1200 turn per minute (rpm) and a constant traverse speed of 50 mm/min; the tilt angle of the pin was 3° towards vertical line; after welding, some samples were prepared in dimensions of $30 \times 30 \times 1.5 \text{ cm}$.

Hardness measurements were done by a diamond lozenge-shape indenter with the load of 0.1 kg for 10 s at cross sections of samples with distances of 1 mm under reference standard of ASTM E384-11. After preparation, some samples of the weld metal were immersed in nitric acid for 20 s to remove the aluminum oxide layers formed on the surface of samples before corrosion test. Electrochemical tests were performed by a three-electrode cell including a calomel reference electrode, a graphite auxiliary electrode, and a working electrode, in a solution of sodium chloride (3.5 wt %) with pH 6.5; the results of those tests were analyzed by Power Suite software under the standard of G102-89.

After immersion of the samples in the mentioned NaCl solution for 30 minutes and reaching a stable potential, the electrochemical impedance test was performed at the open-circuit potential (OCP) in a frequency range of 100 kHz to 10 MHz by using the sinusoidal signal in the potential range of $\pm 1 \text{ mV}$ under the standard of ASTM G106. The potentiodynamic cyclic polarization test was done under the standard of ASTM G59-97. In this test, the primary potential of -0.25 and the final potential of ± 1 were considered

**Fig. 1.** Dimensions used in FSW.

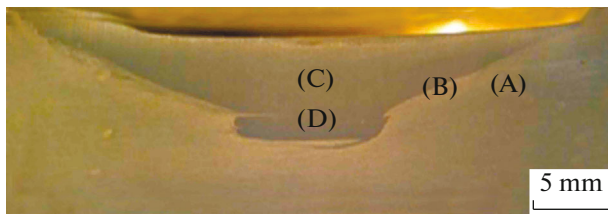


Fig. 2. Microscopic image of cross section of sample welded at 800 rpm and 50 mm/min.

towards the OCP. The cyclic polarization curves were plotted with a scan rate of 1 mV/s; density and equivalent amounts considered were 2.81 and 9.58, respectively.

For macro-etching of samples, a solution including fluoride acid (5 mL), nitric acid (20 mL), hydrochloric acid (20 mL), and 60 mL of distilled water was used for 20 s; a solution including sulfuric acid (2 mL), nitric acid (5 mL), hydrochloric acid (3 mL), and 190 mL of distilled water was used for 30 s to micro-etching of samples.

RESULTS AND DISCUSSION

Microstructure

Figure 2 shows the microscopic image of the cross section of the sample welded at 800 rpm and 50 mm/min, which is free of any defects during welding process such as the tunnel, kiss link, etc. As in [13–15], the cross sections of welded samples (weld metal) were observed in oval and basin-shape. A higher rotating speed to welding speed ratio (high rotating speeds and low traverse speeds) causes the formation of a basin-shape stir zone due to high input heat and more fluent flowing of material around the surface which is in contact with the shoulder. A low ratio of rotating speed to welding speed causes stir zone to be in the shape of lozenge because of low input heat.

Figures 3 and 4 present optical microscopy images of B and C zones from Fig. 2; different welding conditions lead to various microstructures as the grain size of the weld metal. By increasing the tool rotating

speed, the grains were grown and coarsened. If the heat input decreases, then grain refinement will occur. The heat input amount for FSW can be calculated by equation (1) borrowed from [16]:

$$Q = Q = \left(\left(\frac{4}{3} \right) \pi^2 \left(\frac{\eta \mu R_s P r^3}{v} \right) \right), \quad (1)$$

where η is the input heat efficiency, μ is the friction coefficient, R_s is the rotating speed (rpm), v is the traversed speed (mm/min), P is the perpendicular pressure (Pa), and r is the shoulder radius (mm). According to relation (1), decreasing the ratio of the rotating speed to the traversed speed causes reduction of heat input while by increasing this ratio, heat input will be elevated.

Figure 5 presents the grain sizes and distribution of inter-metallic particles of the weld metal of the sample welded at 1000 rpm. As is seen there, the microstructure is fine and coaxial, which is due to dynamic recrystallization occurred as a result of a temperature increase and intense deformation at the welding area. The energy dispersive X-ray spectroscopy results showed two kinds of deposition particles at the microstructure of samples in Figs. 5b, 5c, where the distinction of two kinds of particles is visible. Light vicinities relate to the iron-rich particles and dark areas are the silicon-rich particles.

Observations proved that the grain sizes of each of the three samples have been reduced significantly; as mentioned before, some factors such as dynamic recrystallization and the presence of deposits cause grain refinement; this is why these grains have very small sizes comparing to those of the base metal grains. An increase of the rotating speed that causes enhancement of heat input makes it possible to trigger the grains growth. The dominant parameter against such factors as sediments and dynamic recrystallization is the needed time the grains to grow. At higher rotating speeds, the mentioned time increases too; so, the sample welded at the rotating speed of 1000 rpm was determined as having the optimized grain size. In the case of the samples welded at a rotating speed of 800 rpm, the effective parameter on grain size was the mixing and flowing of the material inside the liquid

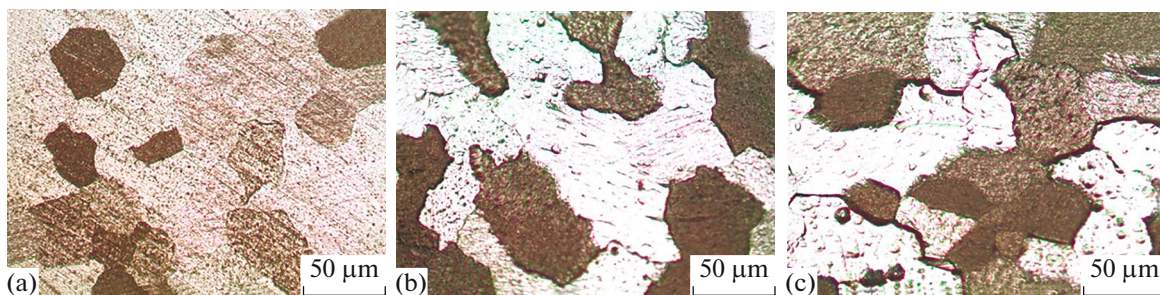


Fig. 3. Optical microscopy images of B zone from Fig. 2: (a) sample at 800 rpm; (b) sample at 1000 rpm; and (c) sample at 1200 rpm.

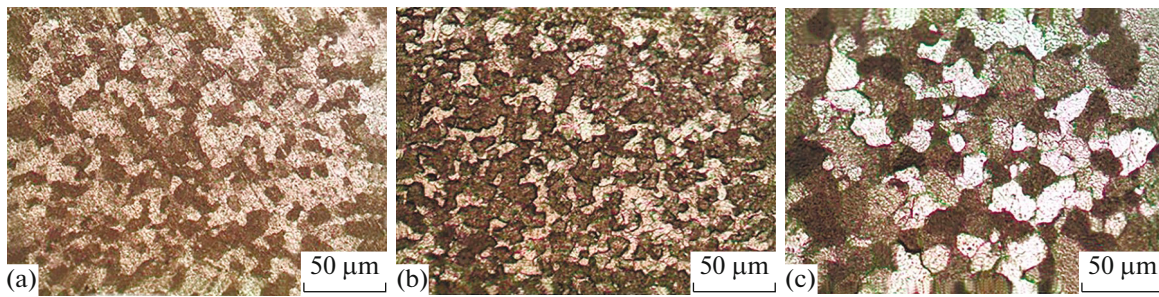


Fig. 4. Optical microscopy images of C zone from Fig. 2: (a) sample at 800 rpm; (b) sample at 1000 rpm; and (c) sample at 1200 rpm.

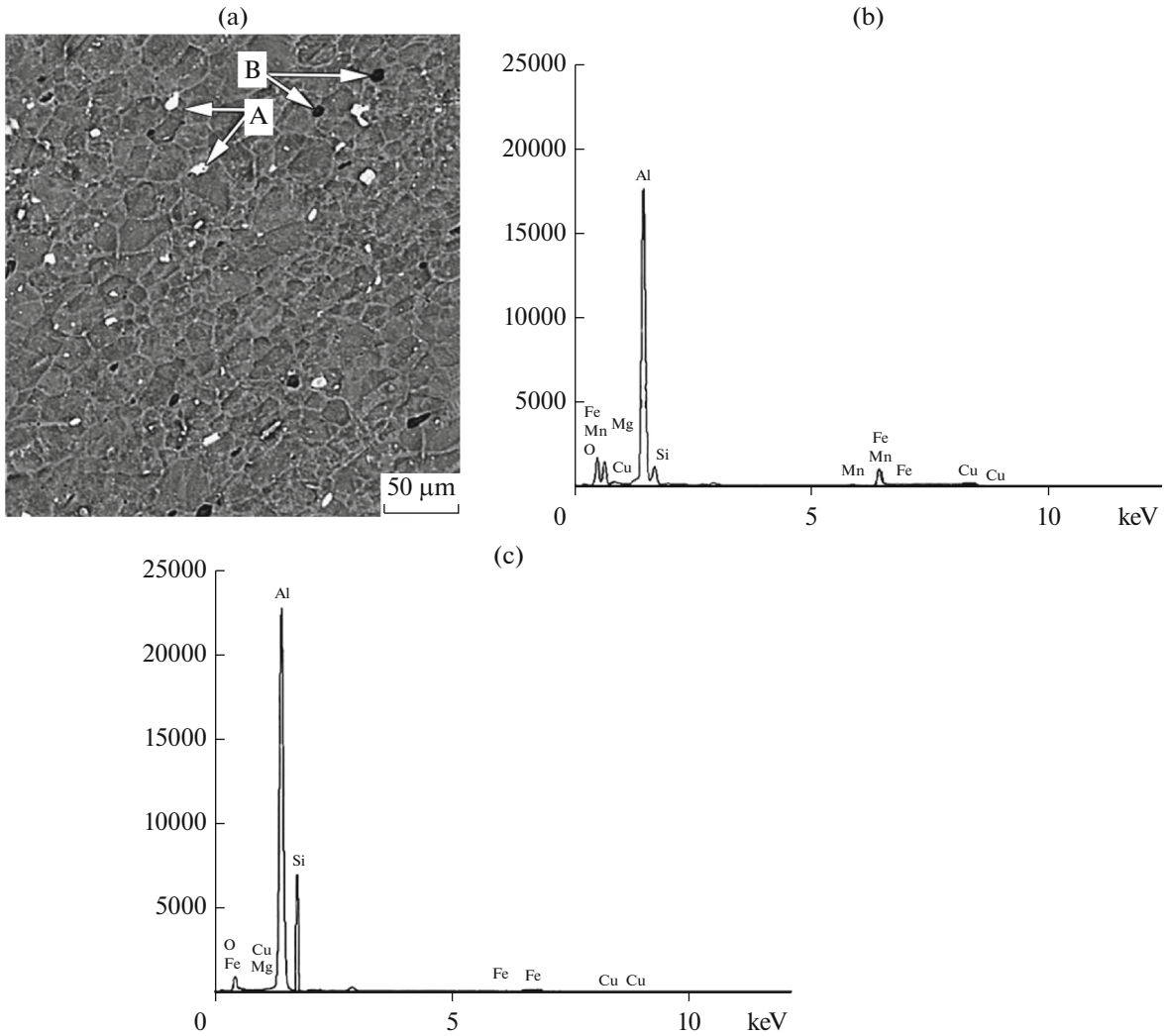


Fig. 5. (a) SEM image of sample welded at 1000 rpm with magnification of 1500 \times ; (b) EDS data on dark deposits; and (c) EDS data on of light sediments.

basin; because of inadequate heat between the tool and the work piece compared to those of the sample with the rotation speed of 1000 rpm, grains have become coarsened [17, 18]. Therefore, the amount of heat, optimized material flowing and stirring (as a result of rotation) in the liquid basin, play a significant role in optimizing the metal properties.

Hardness

According to Fig. 6, the hardest amount at the stir zone occurred for the sample welded at the rotating speed of 1000 rpm. The heat input amount of the sample welded at 800 rpm was not enough for recrystallization; with the sample welded at 1200 rpm, the grain

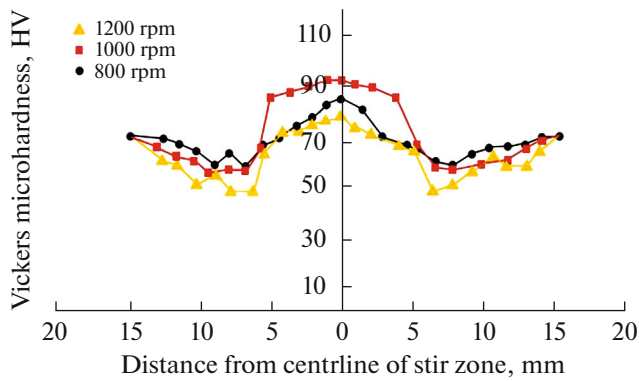


Fig. 6. Hardness diagram of different samples cross sections at various processing conditions.

growth has been improved; but for the sample welded at the rotating speed of 1000 rpm, the proper heat input amount caused recrystallization and prevented grain growth and finally led to the hardness amount drop [19, 20].

Polarization

Figures 7 and 8 present polarization diagrams of the base metal, the weld metal and the HAZ with the used NaCl solution; the related corrosion parameters are given in Table 2.

Figure 7 shows that the alloy passivation did not occur. At the anodic branch in a significant current range, the amount of potential was almost constant and did not change; however, at the cathodic branch, the rate of potential changes was high. As seen in Table 2, β_a was much lower than β_c . Also, the corrosion potential amount was -694.685 , which is in agreement with other investigations [21].

Corrosion current can be converted to corrosion rate (mpy) by the following relation:

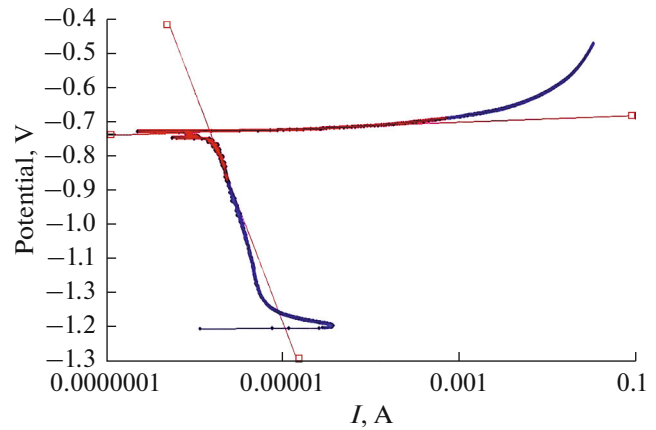


Fig. 7. Polarization diagram of base metal at NaCl solution (3.5%).

$$C.R = 0.129M/ni_{\text{corr}}/D, \quad (2)$$

where M is the atomic mass in g/mole and n is the metallic atom capacity. According to equation (3), the amount of n should be considered as 3:



Corrosion current ($(\mu\text{A})/\text{cm}^2$) is obtained through a polarization diagram. Also, D is the aluminum density in g/cm^3 . The density amount of pure aluminum is $2.7 \text{ g}/\text{cm}^3$. The surface area was 20 mm^2 for all tested samples, so, by substitution of the above data, equation (4) is obtained:

$$C.R = 0.129 \times 27/3i_{\text{corr}}/2.7 = 0.43i_{\text{corr}}. \quad (4)$$

By presenting the relation of (4–3), corrosion rates were calculated for all of the samples whose amounts are given in Table 2.

Against most fusion welding methods, at FSW, the corrosion properties of the weld metal do not decrease compared to those of the base metal; as seen in Figs. 7

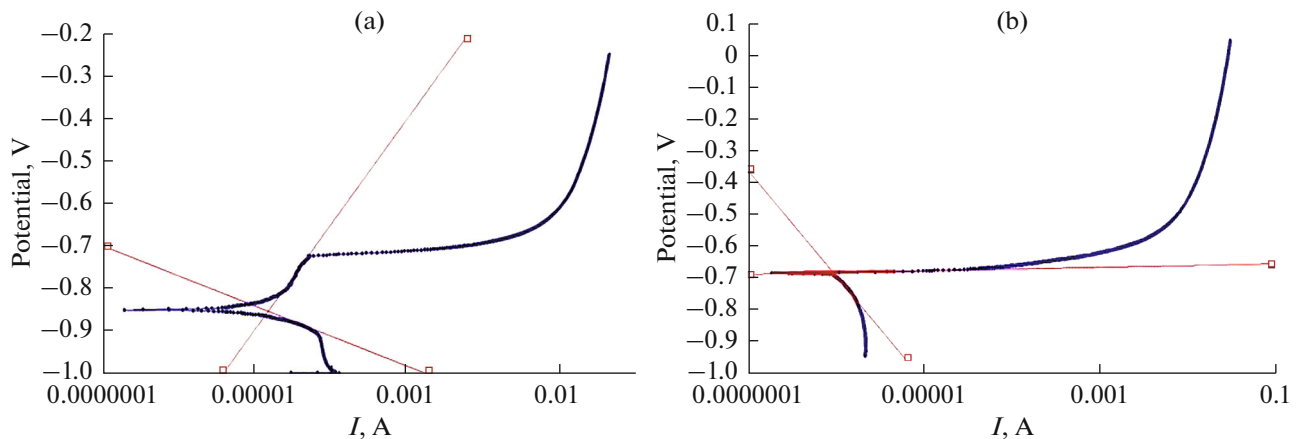


Fig. 8. Polarization diagrams of weld metal in NaCl solution (3.5%); (a) rotating speed 800 rpm, and (b) rotating speed 1200 rpm.

Table 2. Resultant corrosion parameters extracted from polarization tests at chloride solution (3.5%)

	Pin rotation speed, rpm	Corrosion potential, mV	Corrosion current, μA	β_c , mV	β_a , mV	Corrosion rate, mpy
Base metal	—	-694.6	1.55×10^3	607.3	8.861	0.322×10^3
Weld metal	800	-850.7	1.482×10^3	70.8	248.1	0.305×10^3
	1000	-723.896	9.852×10^2	467.636	7.166	0.275×10^3
	1200	-717.598	7.654×10^2	334.496	5.581	0.214×10^3
HAZ	800	-718.750	3.368×10^3	3.707×10^{16}	22.493	0.408×10^3
	1000	-698.19	4.917×10^3	504.141	9.116	0.492×10^3
	1200	-705.876	5.350×10^3	628.986	12.626	0.565×10^3

and 8, the corrosion rate of the weld metal has been lowered compared to that of the base metal. Lack of complete melting at FSW prevents a sharp drop of weld metal properties, but the heat input amount is high enough to cause some changes in metallurgical and mechanical properties of the work piece.

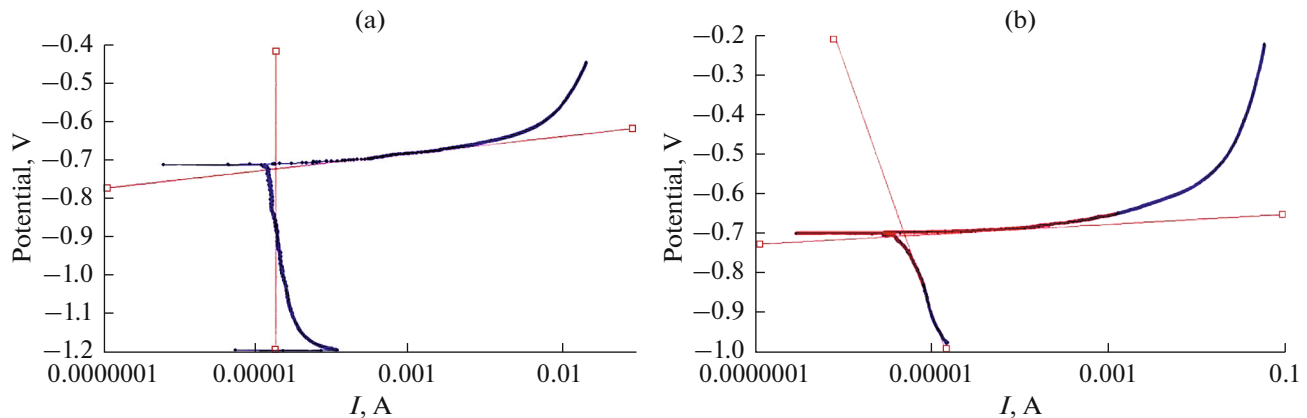
Because of the input heat applied to the weld metal during FSW, the temperature of the metal would increase and deposits will dissolve in the Al. Due to the mechanical and stirring force of FSW, the resultant micro structure will be finer, which can increase the corrosion resistance of the weld metal. These results are in good agreement with those published elsewhere [21–23].

Via increasing the rotating speed at FSW, the heat input amount would also increase and dynamic recrystallization will occur. A higher heat input causes grains and secondary particles growth in the microstructure in addition to dynamic recrystallization. This is the reason of lower weld metal corrosion resistance when the rotating speed increases for the samples in the polarization test. Meanwhile, an increase of the pin rotating speed causes a shift toward more positive and anodic values of the corrosion potential in

polarization diagrams. This matter can be a result of a change in the secondary phase particles ratio in the alloy microstructure. If the amount of the secondary phase is lower in the alloy, then the cathodic reaction amount would decrease during corrosion; so, the diagram shifts to the amounts with a more negative potential.

As shown in Fig. 9, the corrosion rate in the HAZ is higher than that of the base metal and the weld metal. It can be due to an increase of the grain size and the deposition particles size of the secondary phase, which intensifies galvanic corrosion. Thus, increasing the pin rotating speed at FSW causes an increase of the corrosion rate. The main cause of this matter is the enhancement of heat input to the work piece, which, in this case, enhances the heat input to the HAZ, which cause more growth of secondary phase particles.

As seen in the polarization diagram of the HAZ for the sample welded at the rotating speed of 800 rpm (Fig. 9), a lower heat input amount caused by a slower speed of rotating pin leads to a decrease of the corrosion rate compared to that of the base metal. In the samples cut from the HAZ and welded at rotating

**Fig. 9.** Polarization diagrams of HAZ at NaCl solution (3.5%): (a) rotating speed 800 rpm, and (b) rotating speed 1200 rpm.

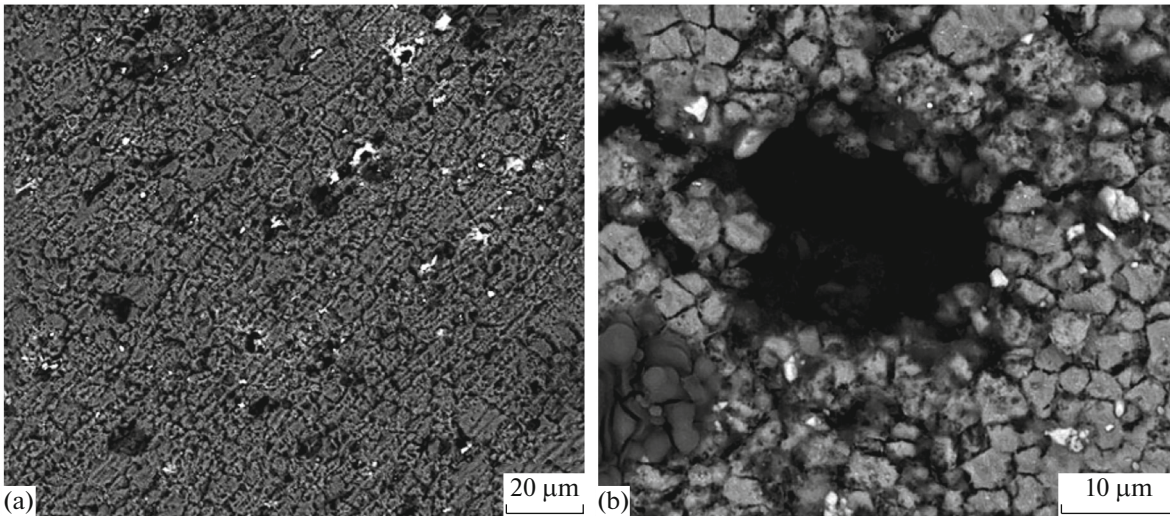


Fig. 10. SEM images of HAZ related to sample with rotating speed 1000 rpm: (a) before corrosion, and (b) after corrosion.

speeds of 1000 and 1200 rpm, an increase of the corrosion rates is quite significant.

SEM images of the HAZ related to the sample with the rotating speed of 1000 rpm are in Fig. 10a—before corrosion and Fig. 10b—after corrosion. Comparing those figures, formation of vast cavities is easily visible after the corrosion test. Therefore, a lower corrosion resistance in the HAZ compared to that of the weld metal is provable, as well.

Electrochemical Impedance

The equivalent circuit used in electrochemical impedance tests is shown in Fig. 11, as obtained by using the z-sim software. The equivalent circuit consists of two electrical resistances: one of them—in series and the other one—in parallel, with a specified constant time.

Q element in the circuit relates to a capacitor. A double electrical layer has a resistance and a capacitor. Capacitors usually do not act uniformly at electrochemical impedance spectroscopy tests and behave as

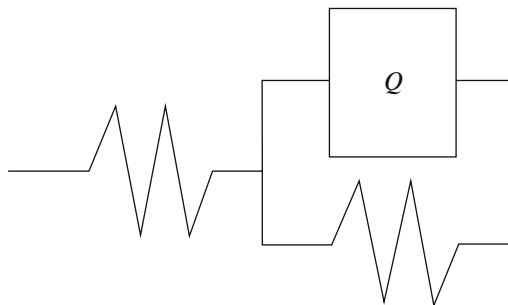


Fig. 11. Electrical equivalent circuit for Al sample at NaCl solution (3.5%).

constant phase capacitors instead. Some theories were suggested to describe the non-ideal behavior of a double electrical layer, but none of them were accepted, completely. For instance, changes in the surface chemical composition and a non-uniform surface composition or surface roughness are efficient in this case.

The electrochemical impedance parameters obtained from the diagram in the Fig. 12 are given in Table 3. The value of n in Table 3 is an ideal amount of capacitor behavior for impedance samples.

As seen, by increasing the pin rotating speed in FSW, the R_p amount in the weld metal (Fig. 13) decreased. So, it can be concluded that the corrosion resistance amount decreases by increasing the pin rotating speed. Figure 14 shows the Nyquist diagram for the haz area at speeds of 800 and 1200 rpm. Also, the corrosion rate in the HAZ was higher than that of the weld metal. This can be because of the growth of grain and of the size of secondary phase deposition particles, which causes more galvanic corrosion.

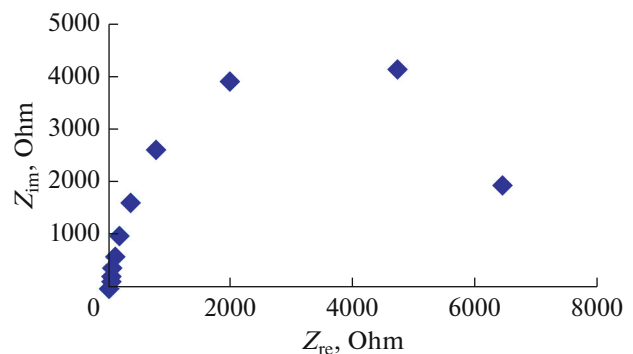


Fig. 12. Nyquist diagram of base metal at NaCl solution (3.5%).

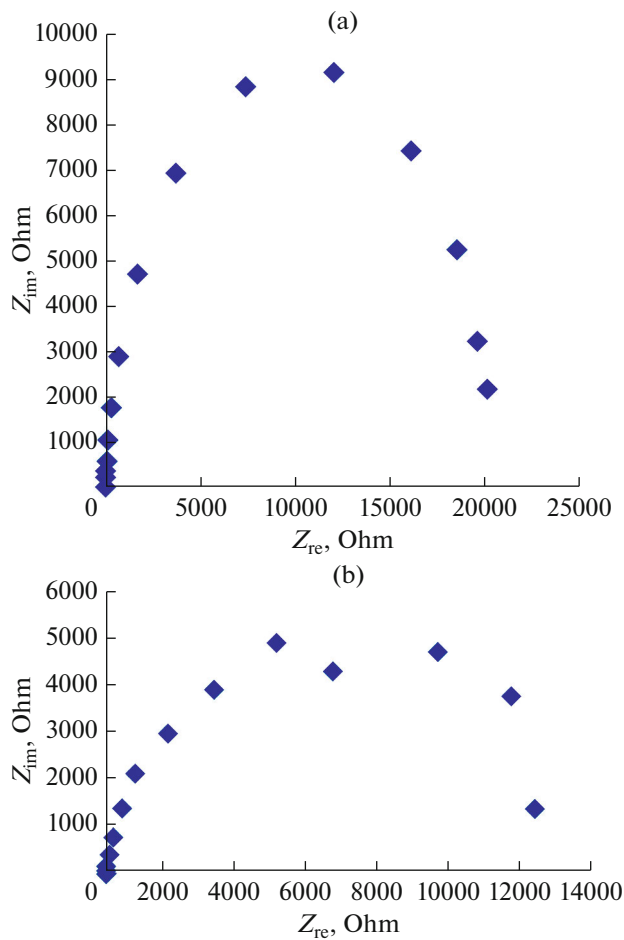


Fig. 13. Nyquist diagrams of weld metal at NaCl (3.5%): (a) rotating speed 800 rpm, and (b) rotating speed 1200 rpm.

Thus, increasing of the pin rotating speed at FSW causes an increase in the corrosion rate. The main cause of this matter is the enhancement of the input heat to the work piece, which, in this case, will cause more intensive growth of secondary phase particles.

Table 3. Resultant electrochemical impedance parameters for weld metal at NaCl solution (3.5%)

Pin rotating speed, rpm	R_S	R	Q	n
—	24.21	10690	1.88E-06	0.93
800	12.28	20330	8.15E-06	0.8
1000	33.61	18340	1.06E-05	0.8
1200	8.593	12490	1.22E-05	0.8
800	7	10670	1.80E-05	0.8
1000	11.11	10170	7.55E-06	0.94
1200	17.95	1564	7.81E-06	0.8

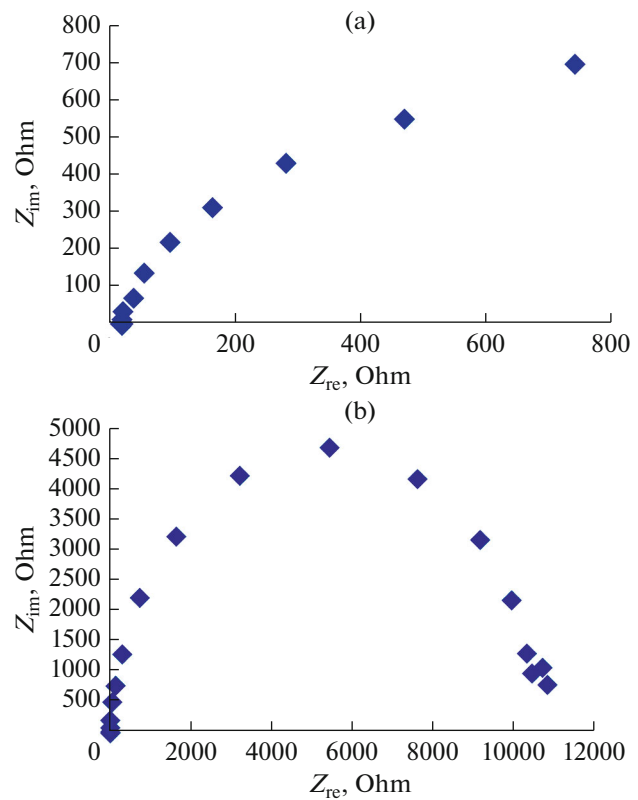


Fig. 14. Nyquist diagrams of HAZ at NaCl solution (3.5%): (a) rotating speed 800 rpm, and (b) rotating speed 1200 rpm.

CONCLUSIONS

From the present research, it can be concluded that:

(1) An increase of the pin rotating speed that causes the enhancement of heat input thus creating an opportunity for grains growth. The needed time for that growth is the dominant parameter against such factors as sediments and dynamic recrystallization. At higher rotating speeds, the mentioned time increased too; so, in the challenge of these parameters, the sample welded at the rotating speed of 1000 rpm was determined as having the optimized grain size.

(2) In the samples welded at the rotating speed of 800 rpm, the effective parameter on the grain size was the stirring and flowing of the material inside the liquid basin. Because of inadequate heat between the tool and the work piece compared to the sample with the rotation speed of 1000 rpm, grains have coarsened. Therefore, the amount of optimized heat input for material flowing and stirring (as a result of rotation) in the liquid basin plays a significant role in optimizing the metal properties.

(3) The hardest amount at stir zone was for the sample welded at the rotating speed of 1000 rpm. The reason relates to the optimized input heat during welding and dynamic recrystallization; so, the grain size

would decrease compared to that of the samples welded at rotating speeds of 800 and 1200 rpm.

(4) The polarization diagram of the weld metal for the sample welded at the rotating speed of 800 rpm, differs from the polarization diagram of the base metal. First, at the anodic branch in a potential range of 100 mV, the behavior is like a passive state, then, the sample behavior becomes similar to that of the base metal. This passivation behavior occurred only at the samples welded at the rotating speed of 800 rpm; the polarization diagram of the samples welded at rotating speeds of 1000 and 1200 rpm had no such an area.

(5) For the sample welded at the rotating speed of 800 rpm, the passive layer formed slowly due to decreasing the presence of the cathodic area, which occurred because of inter-metallic particles dissolving; so, the localized amount of pH would be reduced. During recrystallization of the welded area, the deposits will be formed again. A low amount of heat input causes the refining of formed deposits hence, the galvanic corrosion rate will be decreased.

(6) An increase of the pin rotating speed caused an increase of the corrosion rate in the HAZ; the secondary phase particles growth was identified due to a heat input increase.

(7) The polarization diagram of the HAZ for the sample welded at the rotating speed of 800 rpm showed a lower heat input amount caused by a lower speed of the rotating pin, which leads to a decrease of the corrosion rate amount compared to that of the base metal. While, for the samples cut from the HAZ and welded at rotating speeds of 1000 and 1200 rpm, an increase of the corrosion rate is more significant.

(8) Corrosion amounts of each of the three samples with different rotating speeds relates to the HAZ are almost constant and did not changed so much because recrystallization does not occur at this area.

(9) EIS results indicated that increasing the pin rotating speed at FSW causes reduction of R_p amount at the Nyquist diagram and corrosion resistance.

(10) The Nyquist diagram of the samples welded at the rotating speed of 800 rpm in the HAZ showed that the corrosion rate increase is lower than that of the base metal due to a lower amount of heat input and a lower speed of the rotating pin. Meanwhile, for the samples welded at rotating speeds of 1000 and 1200 rpm, an increase of the corrosion rate is significant in the HAZ area.

REFERENCES

- Cam, G., Guclure, S., Cakan, A., and Serindang, H.T., *Mater. Corros.*, 2009, vol. 4, no. 8, pp. 638–642.
- Taban, E. and Kaluc, E., *Kovove Mater.*, 2005, vol. 45, pp. 241–248.
- Randolph Kissell, J. and Ferry, R.L., *Aluminum Structures: A Guide to Their Specifications and Design*, New York: Wiley, 1995, pp. 10–13.
- Mishra, R.S. and Ma, Z.Y., *Mater. Sci. Eng., R*, 2005, vol. 50, pp. 1–78.
- Thomas, W.M., UK Patent 9125978.8, 1991.
- Singh, R., Rizvi, S.A., and Tewari, S.P., *Int. J. Eng. Trans. A*, 2017, vol. 30, no. 4, pp. 597–603.
- Kumar, S.S. and Ashok S.D., *Procedia Eng.*, 2014, vol. 97, pp. 909–917.
- Thompson, G., *Mater. Sci. Forum*, 1996, vols. 217–222, pp. 95–106.
- Sato, Y.S., Kokawa, H., Enomoto, M., and Jogan, S., *Metall. Mater. Trans. A*, 1999, vol. 30, no. 9, pp. 2429–2437.
- Huang, Y., Wang, Y., Wan, L., et al., *Int. J. Adv. Manuf. Technol.*, 2016, vol. 87, pp. 1115–1123.
- Gharavi, F., Matori, K.A., Yunus, R., Othman, N.K., et al., *J. Mater. Res. Technol.*, 2015, vol. 4, no. 3, pp. 314–322.
- Gharavi, F., Matori, K.A., Yunus, R., and Othman, N.K., *Mater. Res.*, 2014, vol. 17, no. 3, pp. 672–681.
- Elangovan, K. and Balasubramanian, V., *Mater. Sci. Eng., A*, 2007, vol. 459, pp. 7–18.
- Rai, R., De, A., Bhadeshia, H.K.D.H., and Deb Roy, T., *Sci. Technol. Weld. Joining*, 2011, vol. 16, no. 4, pp. 325–342.
- Kimapong, K., Taweekaew, W., and Triwanapong, S., *Key Eng. Mater.*, 2018, vol. 789, pp. 115–119.
- Katsas, S., Todd, G., Jackson, M., Dashwood, R., and Grimes, R., in *Friction Stir Welding and Processing III*, Warrendale, PA: Miner., Met. Mater. Soc., 2005, pp. 292–298.
- Rambabu, G., Balaji Naik, D., Venkata Rao, C.H., Srinivasa Rao, K., and Madhusudan Reddy, G., *Def. Technol.*, 2015, vol. 11, no. 4, pp. 330–337.
- Bhasale, S.R. and Wasekar, M.K., *Int. J. Innovations Eng. Res. Technol.*, 2015, vol. 2, no. 7.
- Zhao, Y., Wang, C., and Dong, C., *Proc. 3rd Int. Conf. on Civil Engineering and Materials Science*, Chengdu: TTP Press, 2018.
<https://doi.org/10.1051/mateconf/201820603002>
- Kaushik, N. and Singhal, S., *Int. J. Microstruct. Mater. Prop.*, 2018, vol. 13, nos. 3–4, pp. 240–255.
- Chouhan, D., Pal, S.K., and Garg, S., *Int. J. Eng. Res. Appl.*, 2013, vol. 3, no. 5, pp. 1972–1978.
- Escalera-Lozan, R., Pech-Canul, M.I., Pech-Canul, M.A., Montoya-Davila, M., et al., *Open Corros. J.*, 2010, vol. 3, pp. 73–79.
- Deepa, P.R. and Rao, P., *Arab. J. Chem.*, 2017, vol. 10, pp. s2234–s2244.